AIAA JOURNAL
Vol. 49, No. 7, July 2011

Scaling Analyses for Large-Scale Space-Based Membrane Optics

Michael J. Shepherd,* Richard G. Cobb,† Anthony N. Palazotto,‡ and William P. Baker§
Air Force Institute of Technology, Wright-Patterson Air Force Base, Ohio 45433

DOI: 10.2514/1.45770

To meet future requirements, space telescopes are envisioned to require primary mirrors that will be on the scale of ≥ 10 m in diameter. Packaging restrictions of current and foreseeable launch vehicles prohibit the use of a single rigid monolithic mirror of that size. Membrane-optics research seeks to create large-diameter apertures out of thin flexible filmlike reflective material. In this analysis, structures with embedded in-plane-actuated piezoelectric elements for active surface shape control were examined. By analyzing the nondimensional form of the governing differential equation, relative effects of linear and nonlinear terms are apparent. Then, through a series of MSC Nastran finite element models, scalability issues are explored to include the effects of nonlinear terms, existing membrane pretension, and unimorph-versus-bimorph actuation. Results show that although small-scale (existing) test articles may respond in accordance with linear models, they may mask the nonlinear characteristics that dominate large full-scale membrane optics in the proposed applications.

Nomenclature

D	=	flexural rigidity (FL)
d_{31}	=	piezoelectric coefficient (LV^{-1})
E	=	Young's modulus ($FL^{-2} = P$)
F	=	fundamental force unit
h	=	mirror thickness (L)
h_p	=	piezoelectric actuator thickness (L)
h_s	=	substrate thickness (L)
L	=	fundamental length unit
l_i	=	length scale (L)
M_P	=	piezoelectric moment forcing (F)
N_O	=	pellicle tension (FL^{-1})
N_P	=	piezoelectric in-plane forcing (FL^{-1})
N_1	=	force intensity (radial) (FL^{-1})
N_2	=	force intensity (hoop) (FL^{-1})
P	=	derived unit (FL^{-2})
P_O	=	tensile pressure ($FL^{-2} = P$)
p_c	=	pressure scale (P)
R	=	radius (L)
r	=	radial coordinate (L)
V	=	difference in electric potential, V
$V(r)$	=	voltage distribution (V)
w	=	out-of-plane displacement (L)
ν	=	Poisson's ratio

I. Introduction

FUTURE requirements for space telescopes are driving the need for development of primary light-gathering mirrors of ≥ 10 m diameter. For nearly all of the current telescope mirrors in use today, the optics are composed of a single rigid monolithic lens or reflector. The diameters of the mirrors currently employed in space telescopes are limited by payload launch constraints on weight and size. For the foreseeable future it will be impractical to package a ≥ 10-m-diam rigid optic for launch. Membrane-optics space telescopes, as shown in Fig. 1, may offer an alternative approach. In this work, the modeling of membrane optics is explored, and observations are made that may guide further research in the design of small-scale laboratory test articles and mathematical simulations that support the goal of creating a large-scale membrane-optics space telescope.

II. Background

A. Scalable Architectures

For most engineering problems of increasing scale, developing a scalable-architecture solution is a good first approach. A *scalable architecture* is defined here as one in which additional performance is gained through the addition of like elements. Scalable architectures have also been proposed by Greshik [1] for the solar sail problem, a challenge that shares many of same design constraints as the space-borne lightweight-optics problem. Figure 2 shows two examples of scalable architectures.

In World War I (WWI), the air war pushed aircraft development at a breakneck pace. A key to maneuverability was the ability of the aircraft wing to generate lift. The biplane was developed, followed by the development of the Sopwith triplane, which in turn had its design borrowed by the German industry to create the famous Fokker Dr.1. This was the scalable-architecture solution in which design teams added additional fabric-covered wings to create lift. The improved lifting performance came at the expense of drag plus added engineering, operational, and manufacturing complexity. As a result, no quad-wing planes were fielded. The postwar period would introduce the monocoque structure, where a metal-stressed wing absorbed the in-flight loads and revolutionized aircraft design and led to increased speeds and maneuverability.

Today, a similar scalable-architecture approach is evident in the James Webb Space Telescope (JWST). The JWST, currently in its final stages of design, uses a primary mirror composed of 18 individual mirror elements, to give it a surface area of 25 m^2, or nearly an order-of-magnitude increase over the Hubble telescope.¶ As with the triplane of WWI, increased system complexity is evident in the control algorithms needed to govern the pointing of the 132-degree-of-freedom actuators that manipulate the JWST mirror system. While the JWST is an undeniable engineering marvel, it remains that rigid mirrors (which comprise the segmented main reflector) can be only made so thin and lightweight. Larger structures made using a

Presented at the IEEE Aerospace Conference with AIAA Technical Sponsorship 2007, Big Sky, MT, 3–10 March 2007; received 1 June 2009; revision received 2 August 2010; accepted for publication 22 September 2010.

*Currently Lieutenant Colonel, Commander, 412th Flight Test Squadron, 300 East Yeager Boulevard, Module 522, Edwards AFB, CA 93525; michael.shepherd@edwards.af.mil. Member AIAA.

†Assistant Professor, Department of Aeronautics and Astronautics, 2950 Hobson Way; richard.cobb@afit.edu. Associate Fellow AIAA.

‡Professor, Department of Aeronautics and Astronautics. Fellow AIAA.

§Associate Professor, Department of Mathematics and Statistics, 2950 Hobson Way.

¶For more information on the James Webb Space Telescope, see http://www.jwst.nasa.gov.

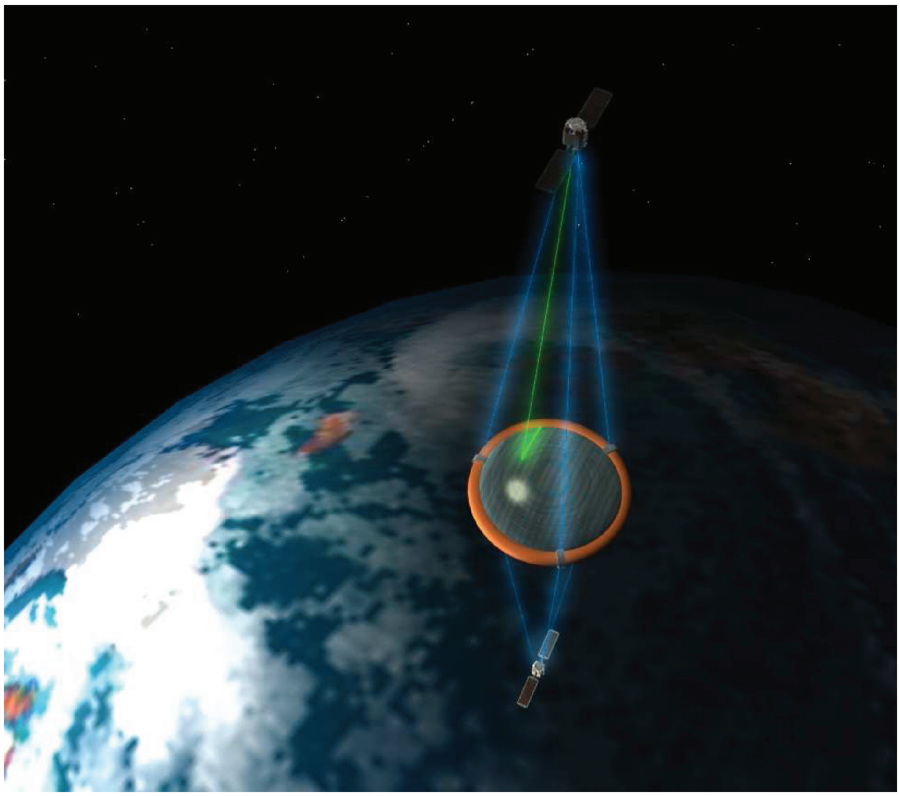

Fig. 1 AFIT on-orbit membrane-optics concept.

similar approach will not appreciably lower the areal density of the light-gathering optics. Just as the WWI biplanes gave way to more modern aircraft designs, for a truly revolutionary increase in space telescope aperture size, another method of manufacture is required.

B. Membrane Optics

There is a proposed alternative to a scalable-architecture approach employed by the JWST, which increases aperture size using a single monolithic structure that is both lightweight and flexible, such that it may be stowed compactly and unfurled. This is the domain of *membrane optics*, in which researchers seek to develop thin-film precision-shaped mirrors on the order of 100 μm in thickness and 10 m or greater in diameter.

One of the early proponents of the membrane-optics space telescope was Ivan Bekey. In his NASA Institute for Advanced Concepts study [2] and later publications [3,4], Bekey proposed the membrane-mirror construction, which forms the basis of this discussion. In the Bekey concept shown in Figs. 3 and 4, a large membrane primary mirror focuses light on a detector array several hundreds of meters from the primary mirror. This was necessary to maintain the advantage of a long focal length when the aperture diameter is increased. In his concept, the word *membrane* is a misnomer: the primary mirror is actually envisioned as a very thin plate with no peripheral frame structure. If not subject to gravitational or solar forces (in the Bekey concept, this is accomplished by orbiting at a Lagrange point and protected by a solar sail), a plate would not need external support. For the Earth-facing space surveillance mission or for interstellar exploratory systems (which may be pointed from one heavenly body to another), a framework for gross tracking control may become a necessity [5]. Once the circumference of the mirror is constrained by a frame, the effects of membrane (or *pellicle*) tension must be considered. Before modeling the system in detail, a discussion of the dimensions involved is warranted.

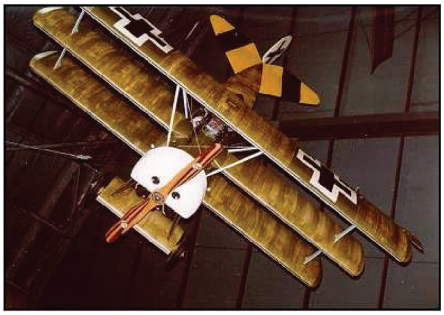

a) WW1 era Fokker Dr.1 triplane photo courtesy of the National Museum of the US Air Force

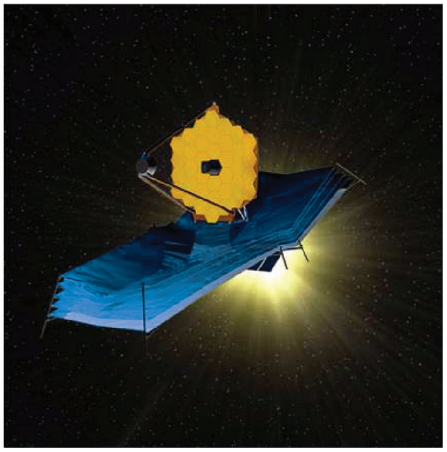

b) JamesWebb Space Telescope illustration courtesy of NASA

Fig. 2 Scalable-architecture examples.

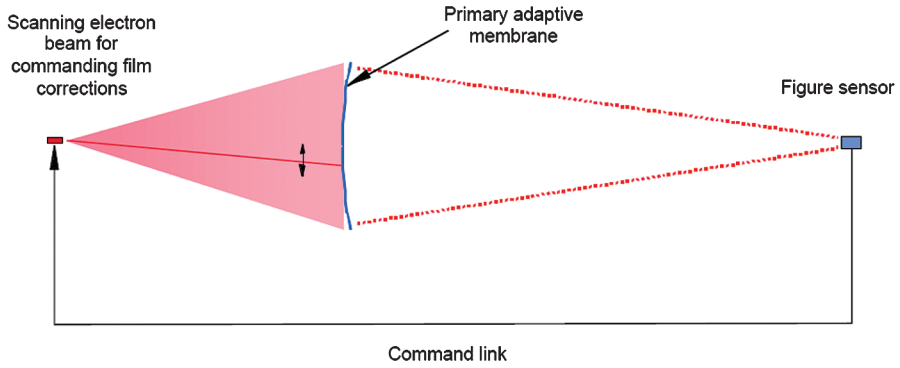

Fig. 3 Bekey concept illustration, courtesy of the NASA Institute of Advanced Concepts.

C. Physical Dimensions for the Space-Based Membrane Optic

In terms of space-based telescope architectures, *large-scale* generally refers to a system with optics in which the aperture diameter is on the order of 10 m. *Small-scale* refers to a scaled-down laboratory test article in which the aperture is on the order of 10 cm in diameter.

Appreciating the order of magnitude of the scales of the problem confronting the engineer is extremely difficult to comprehend. The thickness of membrane optics is about the same as a human hair. If you were to build a skyscraper with a footing the size of the Sears Tower (about 68 m) with the same aspect ratio as the thickness-to-diameter ratio of the membrane-optics mirror, it would reach over 1300 km into the sky and have over 10^6 floors. Further complicating matters is the performance requirement that demands the surface of the membrane optic to conform to shape tolerances of optical (submicron) quality, perhaps even down to tens of nanometers. A familiar analogy is to imagine driving a car around the world on a stretch of highway so smooth that a pothole deeper than a couple of centimeters is never encountered. Thus, membrane optics represent a problem of scale not easily imagined, much less one that must be understood and eventually exploited.

It may be difficult to comprehend the relative sizes in the construction. The f-number, or ratio of focal length to mirror diameter, is 20, which is typical of a space telescope. As a general rule, a space telescope's performance will improve with higher f-number and increased aperture size (mirror diameter).

An equation for the paraboloid surface $w(r)$ of focal length f, radius R, and with radial coordinate r is

$$w(r) = \frac{1}{4f}(r^2 - R^2) \tag{1}$$

To give the reader a physical appreciation for the system, apply Eq. (1) to a hypothetical example in which the notional mirror radius equals 10 m and a focal length of 400 m, the maximum deflection at the center of the paraboloid would be 0.0625 m, or 6.25 cm. The resulting required depression of the paraboloid is less than 1% of the mirror radius. For this reason, insight may be gained by examining the circular plate-membrane structure versus less intuitive paraboloid shell structures. Examination of the plate-membrane structure is also convenient, since manufacturing and packaging techniques may likely begin with a flat-versus-curved surface.

When modeling these systems, it has been common practice to hold all parameters constant, including the thickness of the membrane optic, except for the radius of the membrane itself; scaling a system from a small-scale laboratory experiment to space-based large-scale applications is simply a matter of increasing the membrane's radius. In this work, we find that nondimensionalizing the problem to gain insight and then examining case studies conducted using MSC Nastran finite element analysis may yield a different set of conclusions than from study of small-scale laboratory test articles alone. Before we approach the modeling, let us first examine some of the current work in the field of membrane optics.

D. Previous Work

Researchers have made important contributions to the field of membrane-optics research. Small-scale physical models and experiments for membrane optics have already been successfully demonstrated. Flint et al. [6–8] created a doubly curved membrane shell that may be rolled flat and then released to form a parabolic shape. Mirrors have been constructed with up to meter-class diameters, and the shell's reflective surface has nearly achieved the smoothness required for precision optics. Membrane mirrors with active elements for local and global shaping have been envisioned by many researchers. Electrostatic membrane mirrors are a class of mirrors in which an electrostatic attraction exists between embedded elements in the mirror and the backing structure [9–14]. The

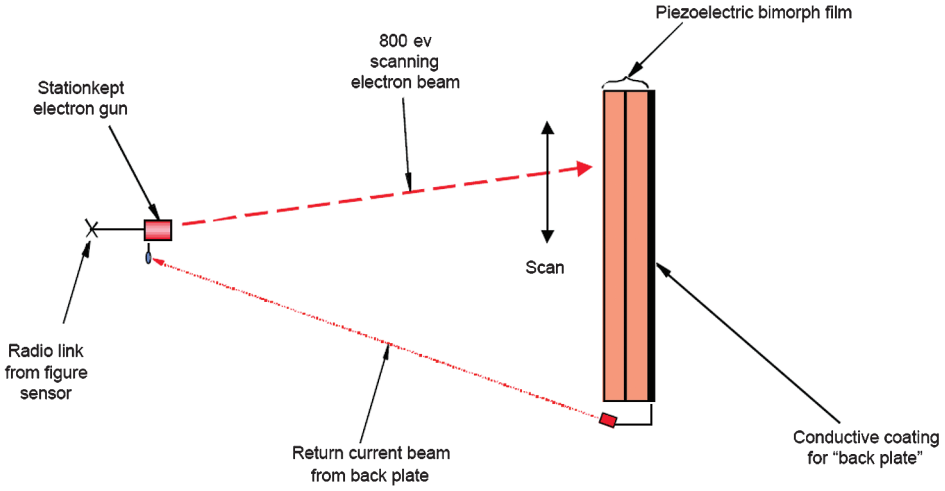

Fig. 4 Bekey concept illustration, courtesy of the NASA Institute of Advanced Concepts.

electrostatic mirror may ultimately be determined to be of limited utility for large-scale telescopes, due to its requirement for a bulky backing structure and the high control voltages needed to induce electrostatic attraction [15].

Unlike the electrostatic mirror, membrane mirrors with embedded piezoelectric elements with unimorph and bimorph internally reacted shaping do not require a backing structure, thus making them ideal candidates for large-scale telescopes. Steinhaus and Lipson [16] and, later, Halevi [17] demonstrated this control methodology on a plate-glass mirror with ceramic PZT (lead zirconate titanate) actuators. Its application to a membrane mirror was presented by Flint et al. [6], where actuators were modeled as line loads. Other modeling by Agnes and Wagner [18] and Rogers and Agnes [19–21] accounted for both the plate- and membranelike qualities of the structure when membrane thickness was introduced, which is an important factor with any internally reacted structure. Fine surface shape control of the mirror is proposed to be achieved through remote actuation of a piezoelectric film by a scanning electron beam that, in theory, can project a voltage film as fine as the beam width. Electron-gun actuation of piezoelectric actuators is a fledgling technology under exploration [22–25].

Experimental work has also progressed. Murphy et al. [26] reported on the development of solar sails for NASA. Their work is unique in that they have tested large membrane structures in as close to a space environment as possible. The difficulties encountered in the testing highlight the need for very accurate scaled models from which conclusions may be drawn, as full-scale testing in a 1 g environment can be extremely difficult, or impossible. On the opposite end of the scale to this application, micromachined deformable-mirror technology using PZT actuators continues to improve, and Hishinuma and Yang [27] reported experimental results showing agreement with an energy-based approach to the microelectromechanical systems problem. Perhaps the most significant experimental work to date was performed by Sumali et al. [28]. The researchers demonstrated a pinned, flat, 80 × 80 mm polyvinylidine difluoride bimorph with a single actuating electrode. The bimorph was approximately 100 μm thick and is precisely the type of construction that is envisioned in this study. Deflections on the order of several hundreds of microns were achieved and were consistent with linear analysis. An example small-scale optical mirror model is the Air Force Institute of Technology (AFIT) deformable-mirror testbed, first reported on by Wagner et al. [29]. The AFIT deformable-mirror testbed, shown in Fig. 5, was a 0.127-m-diam (5-in.-diam), 52-μm-thick, piezoelectric, in-plane-actuated, flat, circular plate-membrane mirror. The mirror is similar to the large-scale optics envisioned in this work. The most recent discussion of the mirror construction and experimental quasi-static control was reported by Shepherd et al. [30]. In that work, the mirror surface was shaped with submicron accuracy and modeled using finite elements. The control algorithms applied were simple linear influence functions that will require refinement to use in the large-scale application. Another small-scale experimental test case by Renno and Inman [31] showed the dynamic response of a 18 in. rectangular strip with piezoelectric bimorph actuation that was accurately modeled with finite elements that introduced piezoelectric tension as a nonlinearity in one of two models. This was a key finding, as it will be demonstrated later in this work that results that were consistent with linear analysis may not be directly extrapolated to large-scale cases. In fact, to develop a space-based membrane telescope, Bekey [2] provided a list of seven key technologies: among them, "determination of the static and dynamic properties of large thin membranes in space, provided with artificial stiffening via piezoelectric action." To this end, an exploration of the governing equations was conducted.

III. Governing Models and Equation

An important first step in the understanding of a membrane optic begins with an analysis of the structure. The word *membrane* itself is something of a misnomer, as it implies that all through-the-thickness properties are negligible. This may be true in the case of an electrostatic membrane, in which pressure forces are applied directly to the mirror's surface, but it is certainly not the case for an in-plane-actuated piezoelectric unimorph or bimorph mirror.

The piezoelectric unimorph or bimorph induces a stress offset from the neutral axis (a term that only has meaning for a plate of finite thickness). For this work, *unimorph* actuation refers to those actuators for which the piezoelectric material is on one side of the neutral axis (normally the nonreflective side for a mirror), and a *bimorph* is one for which the actuators act on both sides of the neutral axis, usually equal in magnitude but opposite in sign.

The governing differential equation for a thin in-plane-actuated structure such as a circular membrane primary mirror may be developed. The following discussion is based purely on the structural response of the mirror to the deterministic forcing of the piezoelectric elements. Other external disturbances such as heating, solar pressure, or body forces induced by gravity were not included. The piezoelectric forces were modeled as equivalent thermal strains based on the work presented by Babuska and Freed [32].

Equation (2) is the partial differential equation at the basis of our analysis for a plate-membrane structure. The equation may be found in any comprehensive text on structural mechanics, such as the text by Nayfeh and Pai [33]. For the following discussion, the static out-of-plane displacement $w(r)$ of an axisymmetric isotropic plate membrane with pellicle tension N_O undergoing in-plane piezoelectric forcing of radius R is [33]

$$D\nabla^4 w(r) - N_O\nabla^2 w(r) + N_P\nabla^2 w(r)\cdots - N_1\left(\frac{\partial w(r)}{\partial r}\right)^2 \frac{\partial^2}{\partial r^2} w(r) - N_2\left(\frac{\partial w(r)}{\partial r}\right)^2 \frac{1}{r}\frac{\partial}{\partial r} w(r)\cdots = -\nabla^2 M_P \tag{2}$$

The individual terms are defined as follows:

$$D = \frac{E(h_p + h_s)^3}{12(1-\nu^2)} \tag{3}$$

$$N_O = (h_p + h_s)P_O \tag{4}$$

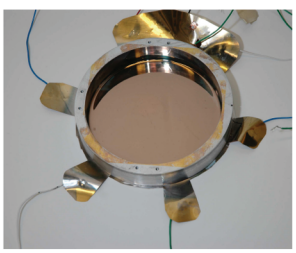

a) Reflective surface of 0.127 meter (2.5 inch) radius mirror

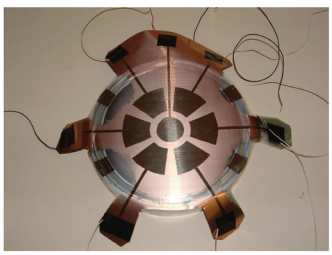

b) Active piezoelectric elements are activated by voltage across electrodes

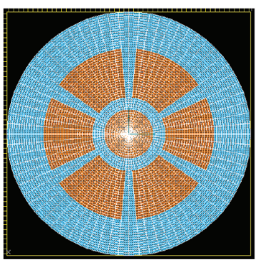

c) Mesh and electrode pattern for piezoelectric actuators used in finite element modeling

Fig. 5 AFIT small-scale deformable-mirror testbed.

$$N_P = \frac{Ed_{31}V(r)}{1-\nu} \tag{5}$$

$$M_P = -\tfrac{1}{2}h_s N_P \tag{6}$$

$$N_1 = \frac{1}{2}\frac{E(h_p + h_s)}{1-\nu^2} \tag{7}$$

$$N_2 = \nu N_1 \tag{8}$$

In the above equations, E is Young's modulus and ν is Poisson's ratio, both terms that are assumed to be the same value for the piezoelectric active material (with thickness h_p) and the inert substrate (with thickness h_s). For certain commonly envisioned constructions such as the structure presented by Williams et al. [34] with a Kapton substrate ($E = 2.55$ GPa and $\nu = 0.34$) and polyvinylidene fluoride (PVDF) active layer ($E = 3.0$ GPa and $\nu = 0.3$), this assumption is not overly restrictive. Consideration for highly pliable incompressible substrates ($\nu \approx 0.5$) or metallic reflective surfaces ($E \approx$ 70 GPa) may require further analysis beyond the scope of this paper.

The familiar plate flexural rigidity D is the result of the Kirchhoff hypothesis. P_0 is the pressure force on the circumference providing the pellicle tension N_O. The piezoelectric moment forcing M_P is a product of the piezoelectric in-plane forcing N_P determined by the piezoelectric coupling matrix coefficient d_{31} and the voltage applied to the piezoelectric layer, $V(r)$. The in-plane force intensity coefficients, N_1 and N_2, result from the integrating the radial and hoop stresses, respectively, through the thickness of the membrane.

Table 1 provides a summary of the terms and units. The terms were expressed in the fundamental units of length L and the derived units of pressure P and voltage V. Although voltage (the difference in electric potential) may often be defined in academic writings as E, it is emphasized in this paper that E represents Young's modulus.

Also note that Eq. (2) corresponds to units of pressure and that the axisymmetric Laplacian operator for this application was

$$\nabla^2 \equiv \frac{\partial^2}{\partial r^2} + \frac{1}{r}\frac{\partial}{\partial r}$$

This problem assumes unimorph actuation. For symmetric bimorph applications, the piezoelectric moment forcing term M_P doubles (h_s replaced by $h_s + h_p = 2h_s$) and the piezoelectric in-plane forcing term N_P vanishes. We may also define the structure thickness as $h = h_p + h_s$.

With the physics of the problem modeled, the next step is to perform a similarity scaling analysis, such that terms of the equation are independent of the units chosen. The problem is nondimensionalized by first scaling the independent variable r and dependent variables w with length scales l_a and l_b and then nondimensionalizing the leading coefficient term by dividing by a scale factor p_c [recalling that Eq. (2) is in units of pressure, we choose p_c to foreshadow the use of a scale factor with the units of pressure that will be required]. Applying the length scales, define the nondimensional variables $\tilde{w} = w/l_a$ and $\tilde{r} = r/l_b$. Then substitute into Eq. (2) and

Table 1 Plate membrane variables and parameters

Variable	Description	Units
r	Radial coordinate (independent)	L
w	Out-of-plane displacement (dependent)	L
P_O	Tensile pressure	P
E	Young's modulus	P
h_s	Substrate thickness	L
h_p	Piezoelectric actuator thickness	L
ν	Poisson's ratio	—
d_{31}	Piezoelectric coefficient	LV^{-1}
$V(r)$	Voltage distribution	V
R	Radius	L

then divide both sides of the equation by the pressure scale p_c to result in

$$\frac{1}{p_c}\left\{D\frac{l_a}{l_b^4}\nabla^4\tilde{w}(\tilde{r}) - N_O\frac{l_a}{l_b^2}\nabla^2\tilde{w}(\tilde{r}) + N_P\frac{l_a}{l_b^2}\nabla^2\tilde{w}(\tilde{r})\cdots - N_1\frac{l_a^3}{l_b^4}\left(\frac{\partial\tilde{w}(\tilde{r})}{\partial\tilde{r}}\right)^2\frac{\partial^2}{\partial\tilde{r}^2}\tilde{w}(\tilde{r})\cdots - N_2\frac{l_a^3}{l_b^4}\left(\frac{\partial\tilde{w}(\tilde{r})}{\partial\tilde{r}}\right)^2\frac{1}{\tilde{r}}\frac{\partial}{\partial\tilde{r}}\tilde{w}(\tilde{r}) = \frac{1}{l_b^2}\nabla^2 M_P\right\} \tag{9}$$

To choose the appropriate scales for this problem, we choose first based upon our intuition. For the scale on the displacement w, we choose the thickness of the material $l_a = h$ as the scale. For the radial term, we would like the problem to be invariant with radius, so we set $l_b = R$. Thus, the radius is normalized, and deflections are terms of multiples of the thickness of the mirror.

To better recognize the equation, we take a moment to rewrite it in simpler terminology. Dropping the tildes, the independent variable, and letting subscripts r and rr indicate the first and second derivatives with respect to r, Eq. (9) becomes

$$\frac{1}{p_c}\left\{D\frac{l_a}{l_b^4}\nabla^4 w + (N_P - N_O)\frac{l_a}{l_b^2}\nabla^2 w\cdots - N_1\frac{l_a^3}{l_b^4}(w_{,r})^2 w_{rr} - N_2\frac{l_a^3}{l_b^4}(w_{,r})^2\frac{1}{r}w_{,r} = \frac{1}{l_b^2}\nabla^2 M_P\right\} \tag{10}$$

Now applying the scales $l_a = h \equiv h_p + h_s$ and $l_b = R$ and choosing $p_c = (h^2/R^2)E$ to cancel as many terms as possible in the nondimensional aspect, we are left with

$$\frac{R^2}{Eh^2}\left\{D\frac{h}{R^4}\nabla^4 w + (N_P - N_O)\frac{h}{R^2}\nabla^2 w\cdots - N_1\frac{h^3}{R^4}(w_{,r})^2 w_{,rr} - N_2\frac{h^3}{R^4}(w_{,r})^2\frac{1}{r}w_r = \frac{1}{R^2}\nabla^2 M_P\right\} \tag{11}$$

With the collection of terms, we write the dimensionless equation as

$$D^*\nabla^4 w + (N_P^* - N_O^*)\nabla^2 w\cdots - N_1^*(w_{,r})^2 w_{,rr} - N_2^*(w_{,r})^2\frac{1}{r}w_{,r} = -\nabla^2 M_P^* \tag{12}$$

where

$$D^* = \frac{1}{12(1-\nu^2)}\frac{h^2}{R^2} \tag{13}$$

$$N_O^* = \frac{P_0}{E} \tag{14}$$

$$N_P^* = \frac{d_{31}V(r)}{h(1-\nu)} \tag{15}$$

$$M_P^* = -\frac{1}{2}\frac{h_s}{h}N_P \tag{16}$$

$$N_1^* = \frac{1}{2(1-\nu)}\frac{h^2}{R^2} \tag{17}$$

$$N_2^* = \nu N_1^* \tag{18}$$

Other scales may be chosen. To examine local conditions such as wrinkles, it may be advantageous to expand the problem by scaling the dependent variable by thickness. However, for this paper we concerned ourselves with the overall global solution. With the

scaling thus now assigned, examination of Eq. (12) yields some interesting findings.

A. Linear Plate

$$D^*\nabla^4 w = -\nabla^2 M_P^* \tag{19}$$

The linear plate model is the simplest model. In this model, no tension is assumed, such as would be the case with a free-edge condition. This is the concept Bekey [2] proposed, in that he imagined a membrane supported only at its center point. The mirror would not be quickly steerable (as Bekey acknowledges), as the inertia term from the dynamic equation of motion (not discussed herein) is large. Alternately, the mirror could be suspended on roller supports at the boundary (perhaps floating in magnetic suspension) to translate and rotate the mirror.

For the linear plate, all nonlinear terms in Eq. (12) are neglected, which is a valid assumption if the slopes of the mirror surface are considered to be small. However, this may not be a good assumption for the large parabolic dishes, as explored in a later section. If the mirror is also to be used for high-spatial-frequency shaping of the received image (such as correcting for Zernike aberrations), the assumption would not hold.

When considering the material properties to be fixed, the effect of altering the diameter or thickness of the linear plate (mirror) can be determined. This might be representative of testing a small-scale structure to see what achievable surface deflection could be obtained with the full-scale structure. To do this, analyze D^* as compared with M^* to find the strength of the forcing as the radius changes. Thus, it may be shown that

$$\frac{M_P^*}{D^*} \propto \frac{R^2}{h^2} \tag{20}$$

Note here that as the radius increases, or as the thickness decreases, the response of the membrane mirror to an applied voltage will be greater; conversely, less voltage will be required for a similar response. This is an encouraging result, as we find that although current piezoelectric material (such as PVDF) have a very small dielectric coefficient (of expansion) d_{31}. Linear theory suggests that large-scale mirrors may not require great loads to create the deformations required. It was such an analysis that allowed Sumali et al. [28] to conclude that linear modeling explained the experimental behavior of their bimorph test article. In the following sections, it will be shown that other terms not present in the linear plate model may dominate the response of large-scale structures.

B. Plate Membrane with Bimorph Actuation

$$D^*\nabla^4 w - N_O^*\nabla^2 w = -\nabla^2 M_P^* \tag{21}$$

In this section, the effect of adding a preexisting tension field to the mirror is discussed. This is the classical membrane tension that gives rise to drumhead dynamics associated with membrane problems.

To analyze this class of problems, the importance of the N_O^* term (the nondimensioned pellicle tension) must be compared with D^* term (the nondimensioned plate stiffness). If D^* is the much-larger term, the effect of N_O^* will attenuate the response of the aforementioned linear plate problem. If D^* is the much-smaller term, it will provide a set of conditions that smooth the membrane response. Figure 6 shows the effect of membrane tension and the demarcation between whether plate stiffness or membrane tension is the dominant term for the dimensioned problem. The figure is provided to emphasize that relatively low tension may significantly impact plate-membrane response as the radius of the mirror increases.

To provide an example, imagine suspending a 0.1-m-radius membrane mirror by five tensioned cables that provide the catenary support. Each cable would then require a force of only 0.01 N before tension would play a central role in the solution. For example, from Fig. 6, at a radius equal to 0.1 m, the demarcation line indicates that N_0 will dominate for values above $N_0 = 0.08$ N/m. Thus, the force

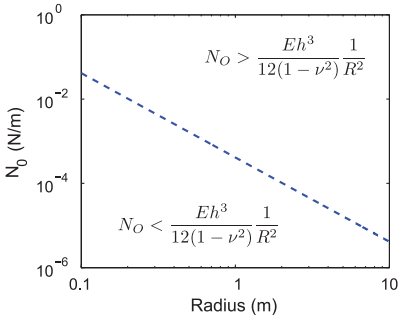

Fig. 6 Tensile load versus radius.

in each cable would need only be 0.08 times circumference, divided by the number of points, or 0.08 N/m$(2\pi 0.1$ m$)/5 = 0.01$ N.

To solve for cases in which either term clearly dominates the other, an asymptotic method may be applied. If $D^* \gg N_O^*$, then divide by D^* to yield

$$\nabla^4 w - \delta^2\nabla^2 w = -\nabla^2 \hat{M}_P^* \tag{22}$$

where $\delta^2 \equiv N_O^*(D^*)^{-1}$ and $\hat{M}_P^* \equiv M_P^*(D^*)^{-1}$. Letting $w = w_0 + \delta^2 w_1 + \cdots$, one can solve the following series of equations by applying the appropriate boundary conditions:

$$\nabla^4 w_0 = -\nabla^2 \hat{M}_P^* \tag{23}$$

$$\begin{aligned} \nabla^4 w_1 &= -\nabla^2 w_0 \\ &\vdots \end{aligned} \tag{24}$$

Apply a similar solution methodology for the cases in which $N_O^* \gg D^*$, and define $\varepsilon^2 \equiv D^*(N_O^*)^{-1}$ and $\bar{M}_P^* \equiv M_P^*(N_O^*)^{-1}$; thus,

$$\varepsilon^2\nabla^4 w - \nabla^2 w = -\nabla^2 \bar{M}_P^* \tag{25}$$

and $w = w_0 + \varepsilon^2 w_1 + \cdots$.

$$\nabla^2 w_0 = -\nabla^2 \bar{M}_P^* \tag{26}$$

$$\begin{aligned} \nabla^2 w_1 &= -\nabla^4 w_0 \\ &\vdots \end{aligned} \tag{27}$$

It is here that an important discovery is made. If a voltage pattern is chosen with a spatial frequency of $f(r/\varepsilon)$, this asymptotic method will not hold true, as all of the terms in the solution will be of the same order.

For cases in which the membrane tension and plate stiffness are of the same order, the solution is more complicated. For the typical case in which the voltage function is simply an indicator (or Heaviside) function corresponding to electrode location, an exact solution for the axisymmetric case can be found as presented by Shepherd et al. [35].

C. Plate Membrane with Unimorph Actuation

$$D^*\nabla^4 w - (N_O^* - N_P^*)\nabla^2 w = -\nabla^2 M_P^* \tag{28}$$

The next system of interest is the plate membrane with unimorph, or single-sided, actuation. This construction is a likely candidate, due to its simplistic nature of construction: only one side of the membrane must be activated.

In the differential equation, the N_P^* term is present, adding a level of complexity to this problem that is not faced with the bimorph construction. This complexity must be carefully treated, because as $-N_P^* \to N_O^*$, the tension term vanishes in that area, and the forcing must balance with the D^* term (the plate stiffness). One also has to be aware that the voltage term that contributes to the N_P^* function may vary along the surface, so the dominance of terms in the equation may

also vary spatially. The practical application in the equation of offsetting tension with piezoelectric forces would be to leave the weak plate term. Under forcing, the structure would likely be subject to buckling and other nonlinear effects.

This may be a significant term for large-scale membrane mirrors with remote actuation. The initial parabolic shape of the membrane mirror would be maintained by applying a constant voltage to the piezoelectric elements. How the piezoelectric term offsets the pellicle tension will be an important design consideration. Fortunately, the construction of large-scale structures should not be limited by the sign of the terms involved. Main et al. [22] experimentally demonstrated the application of positive and negative electric potentials to a piezoelectric with an electron gun by varying the voltage of the backing electrode. We are free to design such that the piezoelectric forces add to the pellicle tension.

D. Nonlinear Plate Membrane

$$D^*\nabla^4 w + (N_P^* - N_O^*)\nabla^2 w \cdots - N_1^*(w_{,r})^2 w_{,rr} - N_2^*(w_{,r})^2 \frac{1}{r} w_{,r} = -\nabla^2 M_P^* \tag{29}$$

The nonlinear effect coefficients N_1^* and N_2^* scale to the same order as the plate-stiffness term D^*. The nonlinear term is especially significant, as one recalls that w is scaled against the plate thickness. That is, for deflections of several centimeters, the nonlinear terms will have the greatest magnitude and the derivative of the surface deflection will be significant. Additionally, if the reflector is deeply curved, or if the surface is actively controlled to create high-spatial-frequency wave-front corrections (such as higher-order Zernike mode shapes), these additional terms must also be included in the analysis. The analytic solution to this problem is not readily available, but the behavior may be examined through the use of finite elements.

IV. Finite Element Examples

A series of finite element examples are presented to demonstrate some of the characteristics of membrane mirrors, as determined from the preceding section.

The finite element model used in these examples was previously presented by Shepherd et al. [36], where the model was evaluated against the AFIT deformable-mirror testbed discussed in Sec. II.D. The model was built using MSC Nastran. For this application, the construction of the finite element model is briefly summarized, with changes from the preceding models detailed.

In this configuration, the model was constructed of 9000 QUAD4 and TRIA3 (plane-strain quadrilateral and triangular) composite plate elements. In this axisymmetric configuration, all azimuthal degrees of freedom were constrained. Linear and nonlinear solvers were used, as called for in the discussion. A hypothetical CTRIA3 element is depicted in Fig. 7.

The model parameters that remained constant throughout the analysis are given in Table 2. The material properties are for a homogeneous mirror composed entirely of PVDF; that is, the electrodes and optical coatings are neglected in this simplified model. The piezoelectric coefficients were implemented similarly to their introduction in Sec. III using the piezoelectric thermal analogy (see Cote et al. [37]).

A nonlinear solution was computed using the SOL 106 strategy, which is called the NLPARM card. The nonlinear parameters were set for up to 50 load increments with the default stiffness update

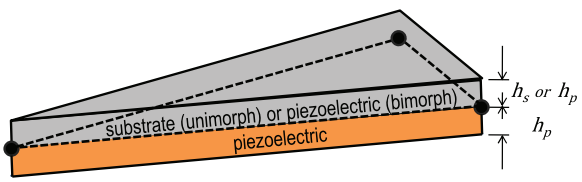

Fig. 7 CTRIA3 plane-strain composite plate element.

Table 2 Finite element model constants

Variable	Description	Value
E	Young's modulus	4×10^9 Nm^2
h	Thickness	104×10^{-6} m
ν	Poisson's ratio	0.3
d_{31}	Piezoelectric coefficient	-2.3×10^{-11} mV^{-1}

method (AUTO). Convergence was set to check load, work, and displacement default criteria. In this manner, the membrane tension was allowed to stiffen the structure through the LGDISP parameter, which allowed geometric changes to the stiffness matrix. Difficulties in convergence due to singularities in the stiffness matrix for structures with high membrane to bending stiffness were overcome by using the parameter K6ROT set to 1.0E6, which introduced a penalty stiffness to the membrane rotation. The loads were applied in two subcases. In the first subcase the pellicle tension was set using the FORCE card applying a load along the edge elements. The second subcase generated the piezoelectric load through the equivalent thermal loads set by TEMPERATURE(LOAD) and TEMPERATURE(INITIAL) cards.

Two actuation patterns for the piezoelectric loads are used in this section. The first forcing function is a smoother application of voltage, defined here as the *drumhead forcing function*, which corresponds to a statically actuated fundamental vibration mode shape for a pure membrane. The applied voltage for this method is

$$V(r) = 300 J_0\left(2.405 \frac{r}{R}\right) \tag{30}$$

where J_0 represents a Bessel function of the first kind.

The second forcing function, *single-electrode forcing*, is similar to the center electrode on the AFIT deformable-mirror testbed in Fig. 5. The voltage patterns are shown in Fig. 8. In the figures, the dependent variables $x = r\cos\theta$ and $y = r\sin\theta$ are used for labeling the x and y axes.

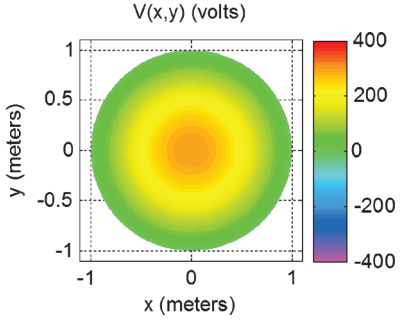

a) Drumhead forcing actuation voltage

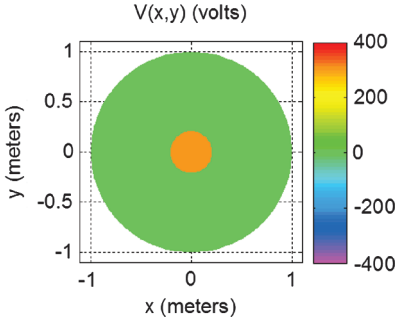

b) Single electrode actuation voltage

Fig. 8 Actuation voltage functions.

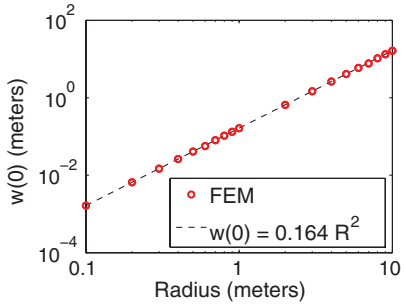

Fig. 9 Center displacement for the linear plate.

A. Linear Versus Nonlinear

The main impetus for this work was to examine the validity of extrapolating the results from a small-scale test mirror to the large-scale mirror sizes in the space telescope application. In particular, previously reported research at AFIT [36] and Sandia National Laboratories [28] showed that small-scale models behaved in accordance with linear models. These small-scale models were of the same thickness/construction as those proposed for the vast sheets to be used in the space telescopes.

Whether applying linear closed-form solution, as used by the researchers at Sandia, or using linear finite element models, the trends will be the same. Figure 9 shows the effect on the linear finite element model of varying a single parameter (the radius) while holding all other dimensions and material properties constant. Figure 9 also shows the out-of-plane displacement of the center node undergoing unimorph actuation by the single-electrode forcing function for a linear plate with clamped boundaries (note that for the linear solver, the introduction of pellicle tension will have no impact on out-of-plane displacement).

From Eqs. (19) and (20), it was observed that D^* will change inversely proportional to R^2, and linear solutions performed analytically or using finite element modeling may be used to confirm this relationship.

Linear solutions are attractive whenever applicable, and one may be tempted to treat 5–10 cm deflections of a 10-m-radius membrane mirror as small and then to apply linear techniques. However, as described in Sec. III.D the nonlinear terms become important in the solution, as when the thickness of the plate is small compared with the radius. This is shown through another series of finite element simulations, this time comparing linear with nonlinear results for different radii. For these examples, the drumhead-forcing-function actuation voltage from Fig. 8a is used (its smooth nature has been qualitatively observed to make the numerical simulations quicker to converge, and it is sufficient for demonstration of the arguments herein). The mirror actuation is the bimorph configuration (eliminating any N_P^* terms) and is held in a roller boundary without any applied pellicle tension (no N_0^* terms). Two cases are presented, each showing a linear and a nonlinear solution. In the first case, a radius of 0.01 m (1 cm) is used to represent a small-scale test article, and in the second case, a 10 m radius is used to represent a space telescope. The results are presented in Fig. 10.

For the 0.01 m case in Figs. 10a and 10b, one may observe that the linear and nonlinear cases present nearly indistinguishable results (in fact, the height of the center out-of-plane displacement is reported as 32.6 μm for the linear case and as 32.0 μm for the nonlinear case, to indicate that the graphs are different). However, changing nothing but the radius to obtain the results in Figs. 10c and 10d tells a completely different story. In Fig. 10c, the scale of the deflection indeed increases by a factor of $R^2 = 10^6$, evident by the scale on the graph, whereas the shape of the plot is identical to the 0.01 m linear case. In contrast, the nonlinear solution is severely attenuated (note the difference in scale compared with the linear solution), and the solution shape does not resemble any of the other three in the figure.

Next, one may return to the issue of scale for an explanation. The terms N_1^* and N_2^* in Eqs. (17) and (18) scale in the same proportion as the plate stiffness with regard to height and radius. Thus, as the plate forces become dominant (increasing ε), the nonlinear term also becomes important. Recall that the out-of-plane displacement $w(r)$ was scaled by the length scale $l_a = h$. Thus, displacements greater than the thickness of the substrate $h = 104$ μm (see Table 2) will be large displacements (and so will the corresponding slope terms) in Eq. (12), further "activating" the nonlinear terms.

It must therefore be concluded that small-scale modeling may not accurately capture the nonlinear effects prevalent in large-scale space telescopes if the thicknesses of the small-scale and large-scale configurations are the same.

B. Plate-to-Membrane Stiffness Effects

In Sec. III.B, preexisting nondimensioned pellicle tension was introduced to the differential equation as N_0^*. In this section, the

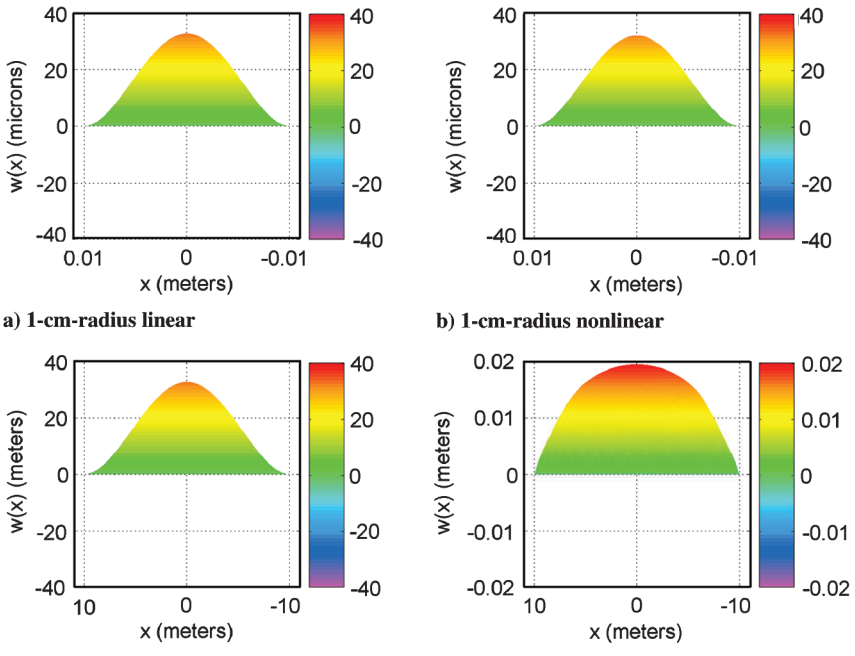

a) 1-cm-radius linear **b) 1-cm-radius nonlinear**

c) 10-m-radius linear **d) 10-m-radius nonlinear**

Fig. 10 Effect of changing radius with different solution strategies.

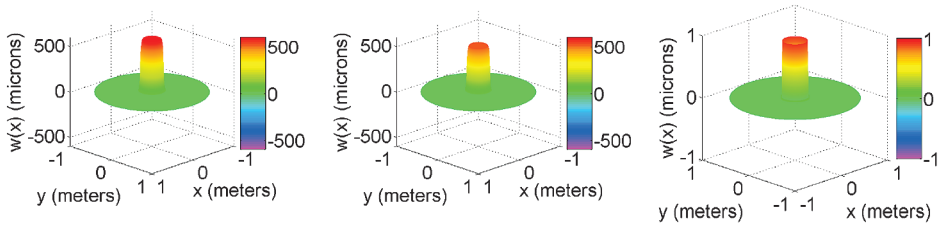

a) $\varepsilon = 1.00$ **b) $\varepsilon = 0.02$** **c) $\varepsilon = 0.0004$**

Fig. 11 Nonlinear solutions for varying ε.

qualitative effect of the ε parameter is presented. Recall that ε is defined as

$$\varepsilon \equiv \frac{D^*}{N_0^*} \tag{31}$$

It is important to remember that the terms above are from the scaled problem. Since the original plate-stiffness term is extremely small, just about any conceivable value of tension would be large, and one might incorrectly assume that the plate-stiffness terms are inconsequential. However, for the small-scale model, one may realize that the plate stiffness is effectively amplified by a factor of R^{-2}. That is, small-scale mirrors in tension will see the effects of plate stiffness much sooner than a large space telescope for a similar tension value.

For the purpose of this comparison, a bimorph mirror of 1 m radius is assumed. Again, the structure is supported by a roller support, with a pellicle tension force added at the boundary. The forcing was introduced with the single-electrode forcing, as shown in Fig. 8b.

Three cases were run in which ε had values of 1, 0.02, and 0.004 (50^0, 50^{-1}, and 50^{-2}) and are presented in Fig. 11. A pure membrane linear solution (one with no plate or nonlinear terms) to the problem would indicate maximum deflections of the center node as a function of ε^2. This relationship was presented in column 2 of Table 3. However, note that the plate-stiffness and nonlinear terms serve to attenuate the pure membrane linear solution.

Again, observe the effects of nonlinear terms. In Fig. 11c, the deflection achieved is on the order of 1000 times less than the thickness h of the mirror; correspondingly, the deflection achieved is near that predicted by the pure membrane linear solution. In Fig. 11b, the deflection is on the same order as the mirror thickness; alternatively, one may note that the deflection is attenuated by nearly half of what the membrane linear theory suggests. Further reductions in tension beyond this level do not lead to increased deflection, as the problem is now a large-deflection problem in which the displacement is limited by the dominance of other terms. This is shown in Fig. 11a.

Finally, the most notable characteristic of the ε term is its influence on the shape of the response. For small ε, as shown in Fig. 11c, the deflection is nearly a scaled (though attenuated) version of the input. This characteristic allows for simplistic surface control algorithms. Again, it is emphasized that it would require a much weaker N_0 term to overcome the plate stiffness as the radius is increased. Effectively, one can conclude that the introduction of pellicle tension (the level of which might be insignificant for small-scale structures) can dominate the surface response on large space telescopes. In fact, if one does not want pellicle tension to dominate the response, care must be taken with the chosen boundary. This may be one reason that Bekey [2] suggests a free-edge condition.

Another interesting observation is made. If the impact of nonlinear terms is sought to be modeled and verified, it should be at the edges of the discrete actuators, where the slope is greatest and their impact will be the most prevalent. Therefore, to analyze the effects of nonlinear terms as observed in Sec. IV.A, which dominate responses of large-scale structures, we should study the behavior, or deflection, of small-scale models with distinct boundary layers. This behavior would be evident at the edges of the electrodes in mirrors constructed similarly to the AFIT deformable-mirror testbed.

Table 3 Center-node deflections for varying ratios of plate stiffness to membrane tension, ε, using different solution techniques

ε	Linear membrane solution	Nonlinear plate-membrane solution
1	4.98 m	590 μm
0.02	1990 μm	518 μm
0.004	0.796 μm	0.797 μm

C. Impact of Unimorph Actuation

A final item worthy of discussion is not a direct result of scaling from small to large structures, but is instead a consequence of lowering the pellicle tension. For structures with low pellicle tension, the unimorph and bimorph actuation techniques will yield differing structural responses. This is especially important, since unimorph actuation is generally regarded as a simpler construct to control, especially when one considers remote-actuation (electron-gun) technologies that are as yet unproven. On the other hand, bimorph applications are easier to model, due to vanishing terms. The N_P^* term in Eq. (12) is only present in the unimorph case and has the ability to dramatically affect the response. To demonstrate its effect, two simulations were conducted. The two cases use unimorph actuation with the drumhead forcing function (Fig. 8a) and the nonlinear solution strategy. The mirror has a 1 m radius and an existing pellicle tension of $N_O = 39.426\ \text{Nm}^{-1}$. When the voltage is applied, its maximum piezoelectric tension is exactly matched in magnitude ($N_P(0) = -39.426\ \text{Nm}^{-1}$). The voltage is applied first as a positive value, and then the same field is applied, but as a negative value. The results are shown in Fig. 12.

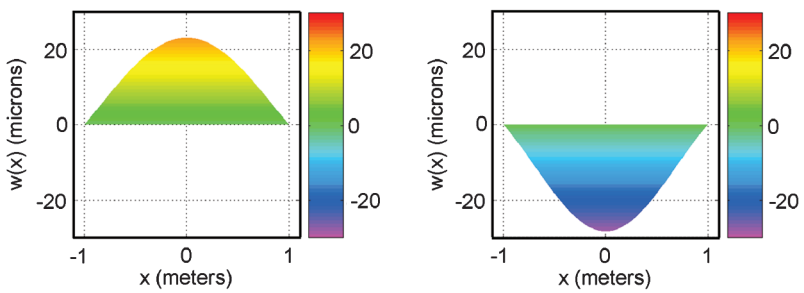

a) Positive-voltage response **b) Negative-voltage response**

Fig. 12 Asymmetric response characteristic of unimorph actuation.

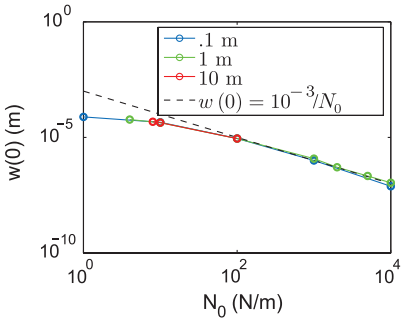

Fig. 13 Center displacement with varying tension.

Figure 12 shows that the absolute value of the displacement is greater when the negative voltage is applied, compared with the positive-voltage case. The simulation shows a deflection of 23.0 μm for the positive-voltage response versus -28.4 μm for the negative-voltage case. To offer a possible explanation, first note that the scaling applied to the problem impacts both terms similarly, as shown in Eqs. (14) and (15), so changes in thickness and radius will have the same impact on each term. What is then observed is that the $(N_P^* - N_0^*)\nabla^2 w$ term in Eq. (12) acts constructively and effectively stiffens the response and limits the deflection. In the second (the negative-voltage) case, the two terms have the same sign and offset each other. Said another way, the pellicle tension is countered by the piezoelectric in-plane force. This offset weakens the overall membrane tension and sets the conditions for an increase in absolute deflection due to the applied moment.

Further evidence of the stiffening effects is shown in Fig. 13. To create this plot, nonlinear finite element simulations were run with the single-electrode forcing function (positive voltage only), and the preexisting pellicle tension N_0 and radius were varied, whereas the other parameters in Table 2 were held constant. The displacement of the center was plotted. Observe the following: at large values of N_0^*, the tension dominates the response and limits the magnitude of the response, such as would be expected in a pure membrane linear solution. The linear response follows the expected curve $w(0) = M_p/N_0$, which is $M_p = 0.001$ for this example and is represented by the dashed line in Fig. 13.

Thus, at large N_0^*, the center deflection varies as $1/N_0^*$. However, at low values of N_0^*, the N_P^* becomes the dominant term in Eq. (12) until the radius is decreased below a reasonable range (at this point, there is little interest in extending results to scale models below the 0.1 m range). For unimorph construction, it was found that the effect of piezoelectric in-plane tension has the potential to dominate the structural response.

The next most obvious question is, what happens when the sign of the voltage is changed and, instead of adding to the existing tension, the tensile field within the area of the piezoelectric material is potentially changed to compression? This is an area of further research. Convergence issues with the finite element model prevent us from displaying results. However, it appears that the model is buckling, and this may prove useful in achieving large deformations with a unimorph structure with low voltage levels and within the realms of current piezoelectric materials.

V. Conclusions

This paper examined the scaling issues associated with the in-plane-actuated deformable mirror for space telescope applications. To gain a better understanding of the problem at hand, the governing differential equation for the axisymmetric system was provided and transformed into a nondimensional form for analysis. To demonstrate some of the pertinent points, a finite element model created in MSC Nastran was created and examined.

Much of the research to date has concentrated on examining small-scale models of membrane optics, where the through-the-thickness construction was assumed to be of the same type as would be used in a large-scale space telescope. However, the radius, or length dimension, was scaled by orders of magnitude. From the examination of the scaled nondimensional equation and demonstrated through the finite element simulations, it was shown that although linear modeling may correctly explain the behavior of small-scale models, only nonlinear models will account for the important terms when the complete large-scale structure is examined. Furthermore, the achievable surface deformations for a large-scale telescope will be far less than those suggested by linear theory, but may still be sufficient to create very shallow, large-focal-length, high-f-number, parabolic membrane mirrors.

For the researcher investigating these technologies, continued reliance on small-scale test articles will be the norm, not the exception. From the results presented, future efforts should be made to try to magnify the nonlinearities that already exist, rather than accepting a linear model that generally seems to model the observed laboratory behavior. This means paying careful attention to preexisting stresses, such as the gravitational body force, if any tension is created in the model. In the small-scale mirror, it was shown that the corresponding deflections are also small. As it is unlikely (without new material breakthroughs) that we will increase the piezoelectric technology to force large deflections, we could instead seek to create sharp discontinuities in the applied voltage by using discrete actuators. In the boundary layer created at the edge of actuators, the effect of nonlinear terms would be amplified, against which models could be verified to later simulate large-scale structures.

By scaling the differential equation, it was observed that the introduction of pellicle (the traditional preexisting membrane) tension may dominate the response of the surface deflections for a large-scale space telescope. Early proposals for space telescopes suggested not using any preexisting pellicle tension; the results herein suggest that if it is introduced, even if it seems to be an intuitively negligible amount, it must also be carefully modeled and examined.

By comparing the strength of terms in the governing differential equation, an unexplored consequence and potential benefit of unimorph versus traditional bimorph in-plane actuation strategies was observed. The unimorph construction introduces a tension field in proportion to the strength of the piezoelectric forcing function that acts on the structure in the same manner as the preexisting pellicle tension field (except that it may be varied in strength as the voltage field varies). In one direction, it was shown that the piezoelectric tension serves to stiffen the structure and attenuate surface deflections. However, it remains as future research to explore the region in which piezoelectric tension places areas of the membrane telescope in compression, and it remains an open area of research to determine if the surface may be buckled into large deflections with low-voltage requirements within the capabilities of current piezoelectric materials and technology.

Acknowledgments

The research presented in this work was conducted with the financial support of the U.S. Air Force Office of Scientific Research under the direction of Sharon Heise. The authors were grateful for the opportunity to present the methods described herein at the 2007 IEEE Aerospace Conference with AIAA sponsorship. The authors would also like to recognize the contributions of the editor and reviewers, whose comments greatly helped to streamline and strengthen this paper.

References

[1] Greschik, G., "Solar Sail Scalability and the Concept of a Truly Scalable Architecture," 47th AIAA/ASME/ASCE/AHS/ASC Structures, Structural Dynamics and Materials Conf., AIAA Paper 2006-1703, Newport, RI, May 2006.

[2] Bekey, I., "An Extremely Large yet Ultralightweight Space Telescope and Array," NASA Institute for Advanced Concepts, Atlanta, 29 May 1999, http://www.niac.usra.edu/files/studies/final_report/58Bekey.pdf [retrieved 2011].

[3] Bekey, I., "A 25 m. Diameter Space Telescope Weighing Less than

150 kg," AIAA Space Technology Conf. and Exposition, AIAA Paper 1999-4478, Albuquerque, NM, Sept. 1999.
[4] Bekey, I., *Advanced Space System Concepts and Technologies*, Aerospace Press, Los Angeles, 2003.
[5] Acikmese, A., Mettler, E., Breckenridge, W., Macenka, S., and Tubbs, E., "L2 Earth Atmosphere Observatory: Formation Guidance, Metrology, and Control Synthesis," AIAA/AAS Astrodynamics Specialist Conf. and Exhibit, AIAA Paper 2004-5212 Providence, RI, Aug. 2004.
[6] Flint, E., Bales, G., Glaese, R., and Bradford, R., "Experimentally Characterizing the Dynamics of 0.5 m Diameter Doubly Curved Shells Made From Thin Films," 44th AIAA/ASME/ASCE/AHS/ASC Structures, Structural Dynamics, and Materials Conf., AIAA Paper 2003-1831, Norfolk, VA, April 2003.
[7] Flint, E., Lindler, J., and Hall, J., "Experimental Validation of Discrete Location Boundary Shape Control for Thin Film Shells," 47th AIAA/ASME/ASCE/AHS/ASC Structures, Structural Dynamics and Materials Conf., AIAA Paper 2006-1903, Newport, RI, May 2006.
[8] Flint, E., Lindler, J., Hall, J., Rankine, C., and Regelbrugge, "Overview of Form Stiffened Thin Film Shell Characteristic Behavior," 47th AIAA/ASME/ASCE/AHS/ASC Structures, Structural Dynamics and Materials Conf., AIAA Paper 2006-1900, Newport, RI, May 2006.
[9] Claflin, E., and Bareket, N., "Configuring an Electrostatic Membrane Mirror by Least-Squares Fitting with Analytically Derived Influence Functions," *Journal of the Optical Society of America*, Vol. 3, No. 11, 1986, pp. 1833–1839. doi:10.1364/JOSAA.3.001833
[10] Wang, P., and Hadaegh, F., "Computation of Static Shapes and Voltages for Micromachined De-Formable Mirrors with Nonlinear Electrostatic Actuators," *Journal of Microelectromechanical Systems*, Vol. 5, No. 3, 1996, pp. 205–220. doi:10.1109/84.536627
[11] Stamper, B., Angel, J., Burge, J., and Woolf, N., "Flat Membrane Mirrors for Space Telescopes," *Proceedings of SPIE*, Vol. 4091, 2000, pp. 126–136. doi:10.1117/12.405771
[12] Stamper, B., Angel, J. R., Burge, J. H., Connors, T., Duffy, B., and Woolf, N., "Stretched Membrane with Electrostatic Curvature (SMEC) Mirrors for Extremely Large Space Telescopes," *Proceedings of SPIE*, Vol. 4451, July 2001, pp. 105–113. doi:10.1117/12.453607
[13] Errico, S., Angel, R., Stamper, B., Burge, J., and Connors, T., "Stretched Membrane with Electrostatic Curvature (SMEC) Mirrors: A New Technology for Large Lightweight Space Telescopes," *Proceedings of SPIE*, Vol. 4849, 2002, pp. 356–364. doi:10.1117/12.457349
[14] Bush, K., German, D., Klemme, B., Marrs, A., and Schoen, M., "Electrostatic Membrane Deformable Mirror Wavefront Control Systems: Design and Analysis," *Proceedings of SPIE*, Vol. 5553, 2004, pp. 28–38. doi:10.1117/12.560521
[15] Tokovinin, A., Thomas, S., and Vdovin, G., "Using 50-mm Electrostatic Membrane Deformable Mirror in Astronomical Adaptive Optics," *Proceedings of SPIE*, Vol. 5490, 2004, pp. 580–585. doi:10.1117/12.550044
[16] Steinhaus, E., and Lipson, S., "Bimorph Piezoelectric Flexible Mirror," *Journal of the Optical Society of America*, Vol. 69, No. 3, 1979, pp. 478–481. doi:10.1364/JOSA.69.000478
[17] Halevi, P., "Bimorph Piezoelectric Flexible Mirror: Graphical Solution and Comparison with Experiment," *Journal of the Optical Society of America*, Vol. 73, No. 1, 1983, pp. 110–113. doi:10.1364/JOSA.73.000110
[18] Agnes, G., and Wagner, J., "Adaptive Structures Technology for Membrane Optical Surfaces," 42nd AIAA/ASME/ASCE/AHS/ASC Structures, Structural Dynamics, and Materials Conf., AIAA 2001-1199, Seattle, WA, Apr. 2001.
[19] Rogers, J., and Agnes, G., "Modeling Discontinuous Axisymmetric Active Optical Membranes," *Journal of Spacecraft and Rockets*, Vol. 40, No. 4, 2003, pp. 553–564. doi:10.2514/2.3977
[20] Rogers, J., and Agnes, G., "Active Axisymmetric Optical Membranes," 43th AIAA/ASME/ASCE/AHS/ASC Structures, Structural Dynamics, and Materials Conf., AIAA 2002-1450, Denver, CO, Apr. 2002.
[21] Rogers, J., and Agnes, G., "Modeling a Piezothermoelastic Beam-String," *Journal of Spacecraft and Rockets*, Vol. 39, No. 5, 2002, pp. 725–731. doi:10.2514/2.3871
[22] Main, J., Nelson, G., and Martin, J., "Electron Gun Control of Smart Materials," *Proceedings of SPIE*, Vol. 3329, Mar. 1998, pp. 688–693. doi:10.1117/12.316942
[23] Nelson, G., Main, J., and Martin, J., "Wavefront Conjugation Using Electron-Gun-Controlled Piezoelectric Materials," *Proceedings of SPIE*, Vol. 4007, Mar. 2000, pp. 582–589. doi:10.1117/12.390344
[24] Hadinata, P., and Main, J., "Time Response of Electron Gun Strain Control of Piezoelectric Materials," *Proceedings of SPIE*, Vol. 3985, Mar. 2000, pp. 378–384. doi:10.1117/12.388839
[25] Hadinata, P., and Main, J., "Survey of Piezoelectric Material Strain Response to Electron Gun Excitation," *Proceedings of SPIE*, Vol. 4327, Mar. 2001, pp. 331–341. doi:10.1117/12.436545
[26] Murphy, D., Macy, B., and Gaspar, J., "Demonstration of a 10-m Solar Sail System," 45th AIAA AIAA/ASME/ASCE/AHS/ASC Structures, Structural Dynamics, and Materials Conf., AIAA Paper 2004-1576, Palm Springs, CA, April 2004.
[27] Hishinuma, Y., and Yang, E., "Piezoelectric Unimorph Microactuator Arrays for Single-Crystal Continuous-Membrane Deformable Mirror," *Journal of Microelectromechanical Systems*, Vol. 15, No. 2, 2006, pp. 370–379. doi:10.1109/JMEMS.2006.872229
[28] Sumali, H., Massad, J., Reu, P., Chaplya, P., and Martin, J., "Analytical and Experimental Studies of Orthotropic Corner-Supported Plates with Segmented In-Plane Actuators," *2005 ASME International Mechanical Engineering Congress and Exposition*, American Society of Mechanical Engineers, New York, Nov. 2005, pp. 197–202. doi:10.1115/IMECE2005-80962
[29] Wagner, J., Agnes, G., and Magee, E., "Optical Metrology of Adaptive Membrane Mirrors," *Journal of Intelligent Material Systems and Structures*, Vol. 11, No. 11, 2000, pp. 837–847. doi:10.1106/F47V-LD4V-4YVR-E13G
[30] Shepherd, M., Cobb, R., Peterson, G., and Palazotto, A., "Quasi-Static Optics-Based Surface Control of an In-Plane Actuated Membrane Mirror," *Journal of Spacecraft and Rockets*, Vol. 44, No. 4, 2007, pp. 953–963. doi:10.2514/1.24847
[31] Renno, D., and Inman, D., "Experimentally Validated Model of a Membrane Strip with Multiple Actuators," *Journal of Spacecraft and Rockets*, Vol. 44, No. 5, 2007, pp. 1140–1152. doi:10.2514/1.27843
[32] Babuska, V., and Freed, B., "Composite Piezoelectric Beam and Plate Elements for Structural Control," 38th AIAA/ASME/ASCE/AHS/ASC Structures, Structural Dynamics, and Materials Conference and Exhibit, AIAA Paper 1997-1312, Kissimmee, FL, April 1997, pp. 1607–1620.
[33] Nayfeh, A., and Pai, P., *Linear and Nonlinear Structural Mechanics*, Wiley Series in Nonlinear Science, Wiley-Interscience, New York, 2004, pp. 408–420.
[34] Williams, B., Inman, D., and Austin, E., "Local Effects of PVDF Patches on Inflatable Space-Based Structures,".
[35] Shepherd, M., Cobb, R., and Baker, W., "Low-order Actuator Influence Functions for Piezoelectric In-plane Actuated Tensioned Circular Deformable Mirrors," *Proceedings of SPIE*, Vol. 6166, Feb. 2006. doi:10.1117/12.658264
[36] Shepherd, M., Peterson, G., Cobb, R., and Palazotto, A., "Quasi-static Optical Control of In-Plane Actuated, Deformable Mirror: Experimental Comparison with Finite Element Analysis," 47th AIAA/ASME/ASCE/AHS/ASC Structures, Structural Dynamics and Materials Conference, AIAA Paper 2006-2231, Newport, RI, May 2006.
[37] Cote, F., Masson, P., Mrad, N., and Cotoni, V., "Dynamic and Static Modelling of Piezoelectric Composite Structures Using a Thermal Analogy with MSC/NASTRAN," *Composite Structures*, Vol. 65, Nos. 3–4, 2004, pp. 471–484. doi:10.1016/j.compstruct.2003.12.008

N. Wereley
Associate Editor